Eur. Phys. J. A (2018) **54**: 141
DOI 10.1140/epja/i2018-12561-y

THE EUROPEAN PHYSICAL JOURNAL A

Regular Article – Experimental Physics

Excitation functions of proton-induced reactions on ^{nat}Fe and ^{nat}Zr targets for the production of cobalt and niobium isotopes

B. Lawriniang[1], S. Badwar[1], R. Ghosh[1], B. Jyrwa[1], H. Naik[2,a], S.V. Suryanarayana[3], and Y.P. Naik[4]

[1] Physics Department, North Eastern Hill University, Meghalaya 793022, India
[2] Radiochemistry Division, Bhabha Atomic Research Center, Trombay, Mumbai 400085 India
[3] Nuclear Physics Division, Bhabha Atomic Research Center, Trombay, Mumbai 400085 India
[4] Product Development Division, Bhabha Atomic Research Centre, Trombay, Mumbai 400085, India

Received: 26 April 2018 / Revised: 8 June 2018
Published online: 28 August 2018

Communicated by R.K. Bhandari

Abstract. Excitation functions of proton-induced reactions for the natural iron and zirconium targets were measured from their respective threshold energies to 22 and 20 MeV. The conventional stacked foil technique was used in combination with the off-line γ-ray spectroscopy at the BARC-TIFR Pelletron facility, Mumbai. The computer code SRIM 2013 was used to calculate the energy degradation along the stack and the proton beam intensity was measured via the ^{nat}Cu(p, x)^{62}Zn monitor reaction. The measured excitation functions were then compared with the literature data available in EXFOR database as well as with the theoretical values from the TALYS-1.8 code and the TENDL-2017 data library. The shapes of the excitation function for all the reactions were reproduced well by TALYS-1.8. In terms of absolute values, for some reactions the data are in good agreement with both the literature data and TALYS-1.8 whereas, for others there is a slight deviation either from the literature data or from the theoretical values of TALYS-1.8 and TENDL-2017.

1 Introduction

Studies on the excitation function of charged-particle–induced reactions are of considerable importance for various practical applications such as thin layer activation, astrophysics, accelerator technology, medical radioisotope production, behavior of materials in particle irradiation and for the development of improved reaction theory. Among different elements iron, zirconium, niobium and aluminum are the primary elements in any accelerator and reactors. Iron is one of the most abundant and most useful metals that make up 5% of the Earth's crust. Stainless steel is an alloy mainly composes of iron, which is highly resistant to corrosion and it can withstand high pressure and temperature. Ferroniobium, an alloy of iron and niobium, is extremely strong and is used in the construction of nuclear reactors. Natural iron has an isotopic composition of ^{54}Fe (5.85%), ^{56}Fe (91.75%), ^{57}Fe (2.12%) and ^{58}Fe (0.28%). On the other hand, zirconium is a metal with five stable isotopes ^{90}Zr (51.45%), ^{91}Zr (11.22%), ^{92}Zr (17.15%), ^{94}Zr (17.38%) and ^{96}Zr (2.80%). The main challenges in designing a reactor [1] consist in specifying the right materials based upon their strength and their interactions with the environment depending upon the metallurgy of the material. The properties of zirconium are, *e.g.*, high melting (1855 °C) and boiling (4371 °C) points, low neutron absorption, good temperature performance and its ability to withstand corrosion of utmost nuclear reactors environment. Thus about 90% of zirconium metal found applications in nuclear reactors. Zirconium metal with addition of niobium [2,3] (containing 1 and 2.5% of niobium) is found to be the right choice to be used as a cladding material of fuel rods in nuclear reactors. Therefore, there is a great demand of highly accurate nuclear data of zirconium as it is one of the important structural materials in the design of the accelerator-driven sub-critical system (ADSs).

The charged-particle–induced reactions of Fe and Zr are also important for the production of radioisotopes for medical purposes, nuclear reactor engineering as well as for other applications. Out of these, nuclear medicine is a rising field in today's generation for detecting and treating diseases like cancer and tumors and the radionuclides are playing a crucial role in this field. The radioisotope ^{90}Nb [4], which is produced by irradiating zirconium with protons, is one of the potential radionuclide

[a] e-mail: naikhbarc@gmail.com (corresponding author)

used in immuno-Positron Emission Tomography (PET). This is because of the short half-life of ^{90}Nb (14.6 hours) produced from the proton irradiation of the high isotopic abundant ^{90}Zr isotope. On the other hand, ^{57}Co radioisotope, obtained by irradiating iron with protons, is used in the Schilling test [5] to test vitamin B-12 deficiency or pernicious anemia [6]. ^{57}Co label to bleomycin (^{57}Co-bleomycin) is used in nuclear scintigraphy [7] for locating and staging lung cancer, in visualizing brain metastases [8] and is also an anti-cancer chemotherapy drug. The ^{56}Co and ^{57}Co radioisotopes are also commonly used as standards for detector calibration [9,10] in γ-ray spectroscopy for high energy ($>$ 1 MeV). The ^{57}Co radioisotope also finds applications in Mossbauer spectroscopy [11] and in Single Photon Emission computed tomography calibration [12] due to its low energy γ-rays.

Among different charged-particle reactions, proton-induced reactions are certainly of interest for accelerator and ADSs. Proton-induced nuclear reactions are also used to produce the radioisotopes for the thin layer activation technique (TLA) [13]. It has been found that the ^{56,57,58}Co and ^{92m}Nb are some of the most suitable radioisotopes for the application of the TLA technique. TLA is performed in order to understand the surface properties of the materials used in nuclear reactors, engineering components and other industrial applications. In view of these facts, in this paper, we focus on the measurements of proton-induced reaction cross sections of iron and zirconium.

In the literature [14–35], it was found that the database for the proton-induced activation on zirconium is scarce and not satisfactory as compared to that of iron. It was also found that there is a large disagreement in the data obtained by different groups of experimentalists. Thus, we study the formation of ^{56,57}Co and ^{90,91m,92m}Nb radioisotopes produced by proton irradiations of iron and zirconium, respectively.

2 Experimental details

The excitation function for the ^{nat}Zr(p, x)^{90,91m,92m}Nb and the ^{nat}Fe(p, x)^{56,57}Co reactions were measured using the 14UD BARC-TIFR [36] (Bhabha Atomic Research Centre and Tata Institute of Fundamental Research) Pelletron facility at Mumbai, India. The proton beam main line at 6 m above the analyzing magnet of the Pelletron facility was used to utilize the maximum proton current from the accelerator. At this port, the terminal voltage is regulated by the generating voltage mode (GVM) using a terminal potential stabilizer. Further, we used a collimator of 6 mm diameter before the target. The experiments were performed by employing the conventional stacked foil activation technique in combination with the off-line γ-ray spectrometry. In these experiments, two separate stacks of iron and zirconium were irradiated with 22 and 20 MeV proton energies, respectively. In the first stack, high-purity ($>$ 99.99%) natural iron and copper metal foils of thickness 100 μm and 103 μm, respectively, were arranged in the order of Al-Fe-Cu-Fe-Cu-Fe-Cu-Fe-Cu-Fe-Cu for irradiation. Similarly, the second stack was arranged in the same way in the order of Zr-Cu-Zr-Cu-Zr-Cu-Zr-Cu-Zr-Cu, in which high-purity ($>$ 99.99%) zirconium and copper metal foils thicknesses of 95 μm and 99 μm, respectively, were used. The sizes of iron and zirconium foils were 0.7×0.7 cm^2 whereas, those of copper foils were 0.8×0.8 cm^2. Copper foils were also included in both stacks to monitor the proton beam intensity as well as to degrade the beam energy. Each foil was wrapped with an aluminum foil of 25 μm thick to avoid contamination from other samples in the stack. The first stack was irradiated for 40 minutes with a proton beam of 21 MeV and beam current of 28 nA. The second stack was irradiated for 10 minutes with a proton beam energy of 20 MeV and beam current of 100 nA.

At the end of irradiations, the stacks were taken out after a considerable cooling time. Then the activated foils were mounted on the Perspex plates and the γ-ray activities were measured with an HPGe detector connected to a PC-based 4 K channel analyzer without chemical separation. In the first few days, γ-ray counting was done at Tata Institute and Fundamental Research (TIFR) and afterwards in the Radiochemistry Division (RCD) laboratory, BARC using two different detectors. Cooling time was required in order to avoid disturbances from overlapping γ-lines of undesired sources. Keeping in mind the half-life of the radionuclides, the samples were counted accordingly in order to get a better counting statistics. Since the half-lives of radionuclides considered here range from 14.6 hours to 271.79 days, measurements started after 2 hours up to 14 days with some time interval. Each sample and monitor foil was recounted three to four times in order to follow the decay of the radionuclides and also for a more accurate evaluation of cross-sections. The irradiated copper monitor foils sandwiched between the samples were counted with the same detector and in a same geometry as the irradiated iron and zirconium samples. The standard ^{152}Eu source [37,38] of known activity was used for the energy and efficiency calibration of the detector. Separate efficiency *versus* energy curves of the detector used at TIFR and RCD, BARC were determined carefully at different source-to-detector distances. From these curves, efficiency values for any gamma line of the produced radionuclides and at various distances could be deduced. The energy resolutions of the detectors were 1.8 keV at the 1332.5 keV γ-line of ^{60}Co. However, the γ-ray countings were done by placing the samples at a distance of about 10–20 cm from the end cap of the detector in such a way that the dead time of the detector was less than 5%.

3 Data analysis

In order to measure the ^{56,57}Fe(p, n)^{56,57}Co and ^{56,57,90,91,92}(p, n)^{90,91m,92m}Nb reaction cross-sections, the proton beam intensity was determined from the ^{nat}Cu(p, x)^{62}Zn monitor reaction, with the known cross-section taken from the IAEA database [39], using the 548.35 and 596.56 keV γ-lines of ^{62}Zn. The protons lose energy as they travel along the stack and this energy degra-

Table 1. Nuclear spectroscopic data for the radionuclides from the $^{nat}Cu(p,x)^{62}Zn$, $^{nat}Fe(p,x)^{56,57}Co$ and $^{nat}Zr(p,x)^{90,91m,92m}Nb$ reactions.

Nuclei	Half-life	Decay mode	γ-ray energy E_γ (keV)	γ-ray intensity I_γ (%)	Production route	Threshold energy (MeV)	Spin parity
^{62}Zn	9.186 h	ε (100%)	548.35	15.3	^{63}Cu(p, 2n)	13.476	0^+
			596.56	26.0			
^{56}Co	77.236 d	ε (100%)	846.77	99.9399	^{56}Fe(p, n)	5.445	4^+
			1238.29	66.46	^{57}Fe(p, 2n)	13.226	
^{57}Co	271.74 d	ε (100%)	122.06	85.60	^{57}Fe(p, n)	1.647	$(7/2)^-$
			136.47	10.68	^{58}Fe(p, 2n)	No threshold	
^{90m}Nb	18.81 s	IT (100%)			^{90}Zr(p, n)	7.096	4^-
					^{91}Zr(p, 2n)	14.370	
^{90g}Nb	14.60 h	ε (100%)	141.18	66.8	^{90}Zr(p, n)	6.971	8^+
			1129.22	92.7	^{91}Zr(p, 2n)	14.245	
^{91m}Nb	60.86 d	IT (96.60%)	1204.67	2.0	^{91}Zr(p, n)	2.167	$(1/2)^-$
		ε (3.40%)			^{92}Zr(p, 2n)	10.898	
^{91g}Nb	6.8×10^2 y	ε (100%)			^{91}Zr(p, n)	2.063	$(9/2)^+$
					^{92}Zr(p, 2n)	10.793	
^{92m}Nb	10.15 d	ε (100%)	934.44	99.15	^{92}Zr(p, n)	2.954	2^+
					^{94}Zr(p, 3n)	18.072	
^{92g}Nb	3.47×10^7 y	ε (100%)	934.5	74.0	^{92}Zr(p, n)	2.818	7^+
		β^- ($< 0.05\%$)			^{94}Zr(p, 3n)	17.936	

dation was calculated using the computer code SRIM-2013 [40], which is based on the energy range relation described by Anderson and Ziegler. However, the loss of proton flux along the stack was negligibly small and therefore it was considered constant in the cross-section calculation given by the activation formula [41]

$$\sigma_R = \frac{A\lambda\left(\frac{CL}{LT}\right)}{N\Phi I_\gamma \varepsilon (1-e^{-\lambda T_i})e^{-\lambda T_c}(1-e^{-\lambda CL})},$$

where A is the net counts in the photopeak, λ is the decay constant ($\lambda = \ln 2/T_{1/2}$) of the reaction product of interest with a half-life $T_{1/2}$, N is the number of target atoms, Φ is the proton flux calculated from the monitor reaction, I_γ is the absolute intensity, ε is the detection efficiency, T_i, T_c, CL and LT are the irradiation, cooling, clock and live times, respectively.

The decay and spectrometric characteristics of the activated products were taken from NuDat [42] database and are presented in table 1 together with the Q-values [43] of the contributing reactions.

4 Results and discussion

The cross-sections for the $^{nat}Fe(p,x)^{56,57}Co$ and $^{nat}Zr(p,x)^{90,91m,92m}Nb$ reactions measured in this work are listed in table 2 and the excitation functions as a function of the proton energy are shown in figs. 1–5. The overall uncertainty was obtained by taking the quadrature sum of statistical and systematic uncertainties. The systematic uncertainties, which summed to 7.8–9.1% are due to uncertainties in proton flux determination ($\sim 6.5\%$), the efficiency detection (1.5–4.9%) and the decay data used (4.0%). The statistical uncertainty due to counting statistic was 1.0–3.8%. Thus, the overall uncertainty was found to range between 7.9% and 9.9%.

For comparison, theoretical calculations of the reaction cross-sections were performed by using the computer code TALYS-1.8 with default parameters as well as by adjusting the level density and optical model parameters. To obtain the best fit the nuclear level density was calculated using the Generalised Superfluid model [44,45] and the optical model parameter was done by adjusting the v_1 parameter of the real volume term as given by Konig and Delaroche [46]. The default and adjusted parameters of different sets of model parameters used in TALYS-1.8 [47] are presented in table 3.

In figs. 1–5, the reaction cross-section obtained for the different reactions were then compared with the literature data available in EXFOR database [48] as well as with the theoretical calculation by the reaction code TALYS-1.8 (default and adjusted parameters) [46] and TENDL-2017 data library [49]. The cross-section increases from zero at the threshold energy to a proton energy, which approaches the Coulomb barrier energy. Then the cross-

Table 2. Experimental cross-sections for the $^{nat}Fe(p,x)^{56,57}Co$ and $^{nat}Zr(p,x)^{90,91m,92m}Nb$ reactions.

Reactions	Threshold Energy (MeV)	$^{nat}Cu(p,x)^{62}Zn$ cross-section σ (mb) [11]	Proton flux $= \times 10^{11}$ p/cm^2	Proton energy (MeV)	Reaction cross-section σ_R (mb)	
					$^{nat}Fe(p,x)^{56}Co$ cross-section σ_R (mb)	$^{nat}Fe(p,x)^{57}Co$ cross-section σ_R (mb)
$^{56}Fe(p,n)^{56}Co$	5.445	45.89	1.40	5.89 ± 1.71	33.13 ± 1.63	6.42 ± 0.83
$^{57}Fe(p,2n)^{56}Co$	13.226			9.73 ± 1.11	342.65 ± 2.23	16.45 ± 2.19
				13.74 ± 0.89	427.27 ± 14.42	8.69 ± 0.82
$^{57}Fe(p,n)^{57}Co$	1.647			16.95 ± 0.88	164.21 ± 22.01	5.55 ± 0.45
$^{58}Fe(p,2n)^{57}Co$	No Threshold			19.99 ± 0.68	60.29 ± 0.19	2.90 ± 0.29
Reactions	Threshold Energy (MeV)	$^{nat}Cu(p,x)^{62}Zn$ cross-section σ (mb) [11]	Proton flux $= \times 10^{11}$ p/cm^2	Proton energy (MeV)	Reaction cross-section σ_R (mb)	
					$^{nat}Zr(p,x)^{90}Nb$	$^{nat}Zr(p,x)^{91m}Nb$	$^{nat}Zr(p,x)^{92m}Nb$
$^{90}Zr(p,n)^{90}Nb$	6.971	39.98	16.8	6.66 ± 1.11	–	11.02 ± 0.73	23.38 ± 0.28
$^{91}Zr(p,2n)^{90}Nb$	14.254						
$^{91}Zr(p,n)^{91m}Nb$	2.167			10.73 ± 0.84	289.42 ± 22.20	37.01 ± 6.49	91.00 ± 3.74
$^{92}Zr(p,2n)^{91m}Nb$	10.897			13.93 ± 0.70	405.01 ± 27.91	78.94 ± 0.98	22.89 ± 0.62
$^{92}Zr(p,n)^{92m}Nb$	2.954			16.69 ± 0.62	388.60 ± 43.30	67.77 ± 1.72	5.46 ± 0.12
$^{94}Zr(p,3n)^{92m}Nb$	17.936			19.15 ± 0.57	217.29 ± 39.64	61.31 ± 7.59	8.04 ± 0.54

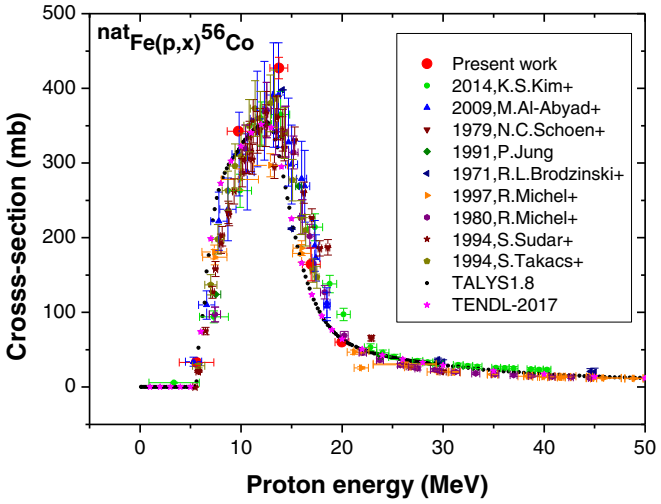

Fig. 1. Excitation function of the $^{nat}Fe(p,x)^{56}Co$ reaction.

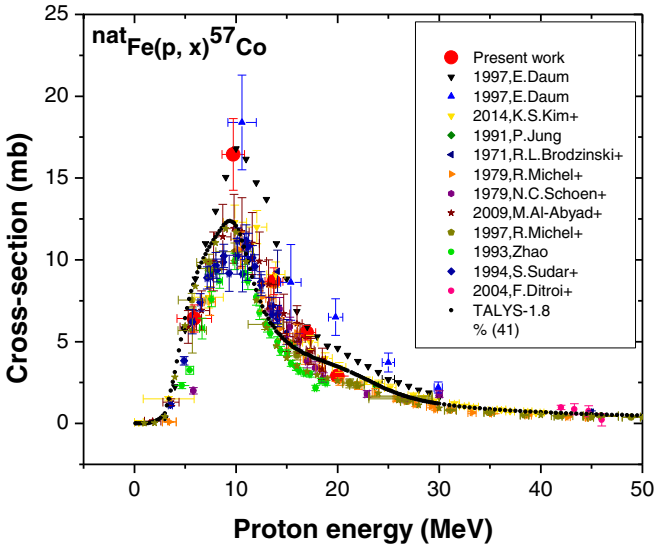

Fig. 2. Excitation function of the $^{nat}Fe(p,x)^{57}Co$ reaction.

section for a particular reaction decreases as more complex nuclear reactions compete.

4.1 $^{nat}Fe(p,x)^{56}Co$ reaction

The long-lived radionuclide ^{56}Co with a half-life of 77.236 days is produced via the $^{nat}Fe(p,x)^{56}Co$ reactions. This radionuclide was identified by γ-lines of 846.77 keV and 1238.29 keV. The excitation function is shown in fig. 1 where the measured reaction cross-section from this work follows the trend of the theoretical prediction by TALYS-1.8 [47] and TENDL 2017 [49] data library. The database for this reaction is very broad. Our experimental data from the present work are in excellent agreement with other literature data except for the proton energy of 13.74 MeV, which is slightly high. The calculation of the $^{nat}Fe(p,x)^{56}Co$ reaction cross-section by TALYS-1.8 calculation with adjusted parameters is found to predict very well the present data.

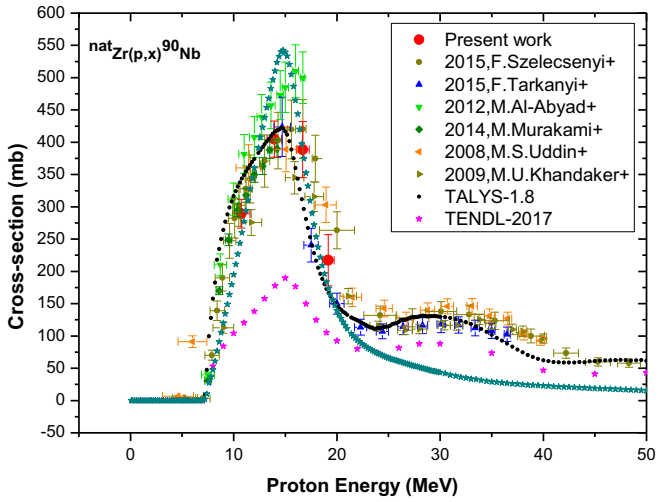

Fig. 3. Excitation function of the $^{\mathrm{nat}}\mathrm{Zr}(\mathrm{p},x)^{90}\mathrm{Nb}$ reaction.

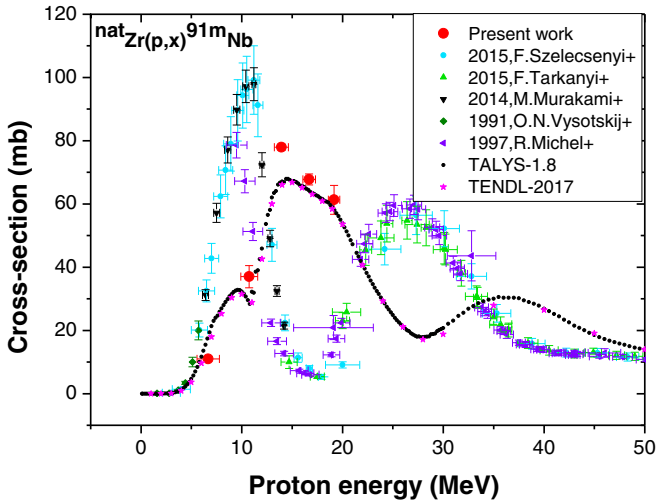

Fig. 4. Excitation function of the $^{\mathrm{nat}}\mathrm{Zr}(\mathrm{p},x)^{91\mathrm{m}}\mathrm{Nb}$ reaction.

4.2 $^{\mathrm{nat}}\mathrm{Fe}(\mathrm{p},\mathrm{x})^{57}\mathrm{Co}$ reaction

The excitation function of $^{\mathrm{nat}}\mathrm{Fe}(\mathrm{p},x)^{57}\mathrm{Co}$ reactions is shown in fig. 2. The excitation function follows the trend of the theoretical calculation by TALYS-1.8 [47]. The magnitudes are in excellent also agreement with the values from TALYS-1.8 as well as with the literature data available in EXFOR [48] database. Our data are well predicted by TALYS-1.8 with the adjusted parameters presented in table 3. As observed in fig. 2, the cross-section values from this work are in excellent agreement with the data by Daum [25], Kim [15], Michel [17], Al-Abyad [30] and Wenrong [26]. However, the cross-section obtained by us at the proton energy of 9.73 MeV is slightly higher in comparison with TALYS-1.8 calculation and other literature data but it is in good agreement with the data by Daum [25].

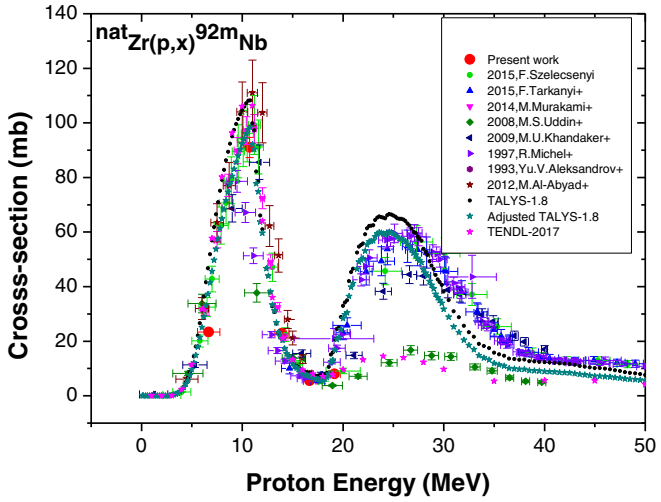

Fig. 5. Excitation function of the $^{\mathrm{nat}}\mathrm{Zr}(\mathrm{p},x)^{92\mathrm{m}}\mathrm{Nb}$ reaction.

4.3 $^{\mathrm{nat}}\mathrm{Zr}(\mathrm{p},\mathrm{x})^{90}\mathrm{Nb}$ reaction

The ground and metastable states of the ^{90}Nb radionuclide have a half-life of 14.6 hours and 18.81 s, respectively. Since the measurement was done after a cooling time of 1.79 hours, the ground state apart from the direct production is also contributed by the internal transition of the isomeric state. Hence the cross-section considered here is the sum of ground and the metastable states. The ^{90}Nb radionuclide was identified by the γ-lines of 141.78 keV (66.8%) and 1129.22 keV (92.7%) for the determination of the reaction cross-section (σ_R). The excitation function of $^{\mathrm{nat}}\mathrm{Zr}(\mathrm{p},x)^{90}\mathrm{Nb}$ reactions from the present experiment is shown in fig. 3 together with the literature data available in EXFOR [48] as well as the calculated values from TALYS-1.8 [47] and TENDL-2017 [49] data library. Over the whole energy range, our data are in good agreement with the literature data by Szelecsenyi *et al.* [27] and Tárkányi *et al.* [28]. The data presented by Al-Abyad *et al.* [30] are a little bit high in the peak region, whereas in the lower range, their data are in agreement with other literature data. The $^{\mathrm{nat}}\mathrm{Zr}(\mathrm{p},x)^{90}\mathrm{Nb}$ reaction cross-section value obtained from TALYS-1.8 [47] based on adjusted parameters is in the acceptable range for both the shape and absolute values.

4.4 $^{\mathrm{nat}}\mathrm{Zr}(\mathrm{p},\mathrm{x})^{91\mathrm{m}}\mathrm{Nb}$ reaction

The excitation function of $^{\mathrm{nat}}\mathrm{Zr}(\mathrm{p},x)^{91\mathrm{m}}\mathrm{Nb}$ reactions is shown in fig. 4. The excitation function obtained in this work is different from the other literature data [17,27–29,33] but it follows the trend of calculated values from TALYS-1.8 [47] using default parameters, moreover the TENDL-2017 [49] data library and the magnitudes are also in good agreement. It is surprising to see from fig. 4 that the peak position of the excitation function of $^{\mathrm{nat}}\mathrm{Zr}(\mathrm{p},x)^{91\mathrm{m}}\mathrm{Nb}$ reactions from the present work, as well as from TALYS-1.8 and TENDL-2017 data library shift towards the higher energy compared to the literature data [17,27–29,33].

Table 3. Default and adjusted parameters used in TALYS-1.8 calculation.

Reactions	Level density			
	Default (γ)	Adjusted (γ)	Default (v_1)	Adjusted (v_1)
^{nat}Fe(p, x)^{56}Co	0.648723	0.99	1.0	0.7
^{nat}Fe(p, x)^{57}Co	0.648723	0.99	1.0	0.7
^{nat}Zr(p, x)^{90}Nb	0.648723	0.99	1.0	3.0
^{nat}Zr(p, x)^{91m}Nb	0.648723	–	1.0	–
^{nat}Zr(p, x)^{92m}Nb	0.648723	0.99	1.0	0.5

4.5 ^{nat}Zr(p, x)^{92m}Nb reaction

The excitation function of ^{nat}Zr(p, x)^{92m}Nb reactions compared with the earlier experimental data available in IAEA database, TENDL-2017 [49] data library and the theoretical calculation by TALYS-1.8 [47] code are shown in fig. 5. As observed in fig. 5, our experimental data show a similar trend as obtained from TENDL-2017 and TALYS-1.8 using default parameters, and the magnitude are also in an acceptable range. The reaction cross-section obtained from TALYS-1.8 with adjusted parameters predicted very well our experimental points and other data available in EXFOR [48] database. It is also observed that our measured data are in excellent agreement with the existing data by Murakami *et al.* [29] over our whole energy range whereas above 10 MeV, they fit well with the data by Al-Abyad *et al.* [30], Tárkányi *et al.* [28] and Michel *et al.* [17].

5 Conclusion

The ^{nat}Fe(p, x)^{56,57}Co and ^{nat}Zr(p, x)^{90,91m,92m}Nb reaction cross-sections have been measured experimentally from the threshold energy up to $\sim$ 20 MeV using the stacked-foil activation technique with an overall uncertainty of about 7.9–9.9%. They are also calculated theoretically by using the nuclear code TALYS-1.8. The experimental results obtained were then compared with the data available in the EXFOR database, TENDL-2017 library as well as with the values from TALYS-1.8. For the ^{nat}Fe(p, x)^{56,57}Co and ^{nat}Zr(p, x)^{90,92m}Nb reactions, the agreement between earlier and present experimental data over the whole investigated energy region is acceptable and hence increases the liability of the database. However, we observed that the cross-section data for the ^{nat}Zr(p, n)^{91m}Nb reaction are different from the literature data but are in good agreement with the TALYS-1.8 calculation and TENDL data library. Since ^{57}Co is a longer-lived radionuclide, it is a good choice for thin layer activation. The proton-induced reaction cross-sections are minimal as compared to neutron-induced reactions and hence the measured data could play an important role to enrich the literature database leading to various practical applications and for improving the models and adjusting input parameters.

We would like to thank the operating staffs of Tata Institute Fundamental Research, Mumbai for their kind help and invaluable assistance in operating the accelerator during irradiations. One of the authors (BL) also gratefully acknowledges the financial support of the UGC for her PhD work.

References

1. https://www.iaea.org/About/Policy/GC/GC51/GC51InfDocuments/English/gc51inf-3-att7_en.pdf.
2. *Nuclear Power Plant Design Characteristics: Structure of Nuclear power plant design characteristics in the IAEA power reactor information system (PRIS)* (IAEA, Vienna, 2007) IAEA-TECDOC-1544, ISBN 92–0–102507–6, ISSN 1011–4289.
3. A.V. Nikulina, Met. Sci. Heat Treat. **45**, 7 (2003).
4. V. Radchenko, H. Hauser, M. Eisenhut, D.J. Vugts, G.A.M.S. van Dongen, F. Roesch, Radiochim. Acta **100**, 875 (2012).
5. A. Murphy, J. Maisterrena, J. Labardini, J.A. Ruiz, C. Luviano, Rev. Invest. Clin. **43**, 346 (1991).
6. http://ntips4u.blogspot.in/2009/01/diagnostic-and-therapeutic-uses-of.html.
7. https://www.rug.nl/research/portal/files/3418635/oenieweg.PDF.
8. O. Nieweg, D.A. Piers, H. Beekhuis, Clin. Neurol. Neurosurg. **90**, 109 (1988).
9. R.L. Auble, W.C. McHarris, W.H. Kelly, Nucl. Phys. A **91**, 225 (1967).
10. https://www-pub.iaea.org/MTCD/publications/PDF/Pub1287_Vol1_web.pdf.
11. https://serc.carleton.edu/research_education/geochemsheets/techniques/mossbauer.html.
12. E.E. Sapir, L. Bettman, G. Iosilevsky, D. Milshtein, A. Frenkel, G.M. Kolodny, S.B. Haim, O. Israel, D. Front, J. Nucl. Med. **35**, 1129 (1994).
13. K. Abbas, D. Gilliland, M.F. Stroosnijder, Appl. Radiat. Isot. **53**, 179 (2000).
14. R. Ghosh, S. Badwar, B. Lawriniang, B. Jyrwa, H. Naik, Y. Naik, S. Suryanarayana, S. Ganesan, Nucl. Phys. A **964**, 86 (2017).
15. K.S. Kim, M.U. Khandaker, H. Naik, G. Kim, Nucl. Instrum. Methods Phys. Res. B **322**, 63 (2014).
16. M. Al-Abyad, M.N.H. Comsan, S.M. Qaim, Appl. Radiat. Isot. **67**, 122 (2009).

17. R. Michel, R. Bodemann, H. Busemann, R. Dam, M. Gloris, H.-J. Lange, B. Klug, A. Krins, I. Leya, M. Liipke, S. Neumann, H. Reinhardt, M. Schnatz-Biittgen, U. Herpers, Th. Schiekel, F. Sudbrock, B. Holmqvist, H. Cond, P. Malmborg, M. Suter, B. Dittrich-Hannen, P.-W. Kubik, H.-A. Synal, D. Filges, Nucl. Instrum. Methods Phys. Res. B **129**, 153 (1997).
18. S. Sudar, S.M. Qaim, Phys. Rev. C **50**, 2408 (1994).
19. S. Takacs, L. Vasvary, F. Tarkanyi, Nucl. Instrum. Methods Phys. Res. B **89**, 88 (1994).
20. P. Jung, EXFOR, Conf. Proc. 91JUELIC 352 (1991).
21. R. Michel, G. Brinkmann, J. Radioanal. Chem. **59**, 467 (1980).
22. N.C. Schoen, Phys. Rev. C **20**, 88 (1979).
23. R. Michel, G. Brinkmann, H. Weigel, W. Herr, Nucl. Phys. A **322**, 40 (1979).
24. R.L. Brodzinski, L.A. Rancitelli, J.A. Cooper, N.A. Wogman, Phys. Rev. C **4**, 1257 (1971).
25. E. Daum, *Investigation of light ion induced activation cross sections in iron. Proton induced activation cross sections*, Progress Report No. NEA/NSC/DOC(97)13 INDC(GER) 043, 4-8 (1997).
26. Z. Wenrong, L. Hanlin, Y. Weixiang, Chin. J. Nucl. Phys. **15**, 337 (1993).
27. F. Szelecsényi, G.F. Steyn, Z. Kovács, C. Vermeulen, K. Nagatsu, M.R. Zhang, K. Suzuk, Nucl. Instrum. Methods Phys. Res. B **343**, 173 (2015).
28. F. Tárkányi, F. Ditrói, S. Takács, A. Hermanne, M. Al-Abyad, H. Yamazaki, M. Baba, M.A. Mohammad, Appl. Radiat. Isot. **97**, 149 (2015).
29. M. Murakami, H. Haba, S. Goto, J. Kanaya, H. Kudo, Appl. Radiat. Isot. **90**, 149 (2014).
30. M. Al-Abyad, A.S. Abdel-Hamid, F. Tarkanyi, F. Ditroi, S. Takacs, U. Seddik, I.I. Bashter, Appl. Radiat. Isot. **70**, 257 (2012).
31. M.U. Khandaker, K. Kim, M.W. Lee, K.S. Kim, G.N. Kim, Y.S. Cho, Y.O. Lee, Appl. Radiat. Isot. **67**, 1341 (2009).
32. M.S. Uddin, M.U. Khandaker, K.S. Kim, Y.S. Lee, M.W. Lee, G.N. Kim, Nucl. Instrum. Methods Phys. Res. B **266**, 13 (2008).
33. O.N. Vysotskij, A.V. Gonchar, O.K. Gorpinich, S.N. Kondratev, V.S. Prokopenko, S.B. Rakitin, V.D. Skljarenko, V.V. Tokarevskij, EXFOR, C 91MINSK, 486 (1991).
34. Y.V. Aleksandrov, S.K. Vasiliev, R.B. Ivanov, M.A. Mikhailova, T.I. Popova, V.P. Prikhodtseva, A.A. Astapov, A. Kolachkovsky, P. Misiak, A.F. Novgorodov, EXFOR, C 93DUBNS, 406 (1993).
35. F. Ditrói, F. Tárkányi, J. Csikai, M.S. Uddin, M. Hagiwara, M. Baba, AIP Conf. Proc. **769**, 1011 (2004).
36. BARC–TIFR Pelletron-LINAC Facility, Silver Jubilee (1988–2013), available at `www.tifr.res.in/~pell/plf25_2013.pdf`.
37. I.A. Alnour, H. Wagiran, N. Ibrahim, S. Hamzah, W.B. Siong, M.S. Elias, AIP Conf. Proc. **1584**, 38 (2014).
38. A.W. Tyler, Phys. Rev. **56**, 125 (1939).
39. `http://www-nds.iaea.org/medical/monitor_reactions.html`.
40. J.F. Ziegler, Nucl. Instrum. Methods Phys. Res. B **219-220**, 1027 (2004).
41. G. Gilmore, J.D. Hemingway, *Practical Gamma-Ray Spectrometry* (John Wiley and Sons, England, 1995) p. 17.
42. *NuDat* 2.7β, National Nuclear Data Center, Brookhaven National Laboratory, updated 2011, available on `https://www.nndc.bnl.gov/nudat2/(updated)`.
43. *Q-value*, `cdfe.sinp.msu.ru/services/calcthr/calc_thr.html`.
44. A.V. Ignatyuk, K.K. Istekov, G.N. Smirenkin, Sov. J. Nucl. Phys. **29**, 450 (1979).
45. A.V. Ignatyuk, R. Capote, *Nuclear Level Densities*, in *Handbook for Calculations of Nuclear Reaction Data*, RIPL-2, IAEA-TECDOC-1506, 85 (2006).
46. A.J. Koning, J.P. Delaroche, Nucl. Phys. A **713**, 231 (2003).
47. A.J. Koning, *TALYS user manual, A nuclear reaction program, User manual*, NRG-1755 ZG PETTEN, The Netherlands (2015).
48. IAEA-EXFOR Data base at `http://www.nds.iaea.org/exfor`.
49. A.J. Koning, D. Rochman, Nucl. Data Sheets **113**, 2841 (2012).